ECS Transactions, 91 (1) 1751-1760 (2019)
10.1149/09101.1751ecst ©The Electrochemical Society

Synthesis and Evaluation of the *A*–site Deficient Perovskite $La_{0.65}Sr_{0.3}Cr_{0.85}Ni_{0.15}O_{3-\delta}$ as Fuel Electrode for High Temperature Co–electrolysis Enhanced by *In Situ* Exsolution of Ni Nanoparticles

D. M Amaya Dueñas[a]*, G. Chen[b], A. Weidenkaff[c], N.Sata[a], F.Han[a], G. Schiller[a], R. Costa [a]*, A.K. Friedrich [a]

[a] German Aerospace Center (DLR), Institute of Engineering Thermodynamics
Pfaffenwaldring 38-40, D-70569 Stuttgart, Germany
[b] University of Stuttgart, Institute for Materials Science
Heisenbergstraße 3, D-70569 Stuttgart, Germany
[c] Fraunhofer IWKS, Materials Recycling and Resource Strategies
Brentanostraße 2a, D-63755 Alzenau, Germany
*corresponding authors: diana.amayaduenas@dlr.de, remi.costa@dlr.de

Lanthanum strontium chromite (LSC) perovskite partially doped with 15% of Ni on the *B*-site as reducible transition metal was investigated with the aim to perform *in situ* exsolution under reducing conditions. *A*-site deficient compounds were formulated to enhance the exsolution of the electrocatalyst. Single phase is achieved with the formulation $La_{0.65}Sr_{0.3}Cr_{0.85}Ni_{0.15}O_{3-\delta}$ (L65SCN) and has been characterized by X–ray diffraction (XRD), Rietveld refinement and scanning electron microscopy (SEM). Exsolution was investigated under reducing conditions in which Ni exsolution was confirmed. Such electrocatalyst was implemented into an electrolyte-supported-cell (ESC) for early electrochemical investigation. Cells were manufactured by screen printing of composite L65SCN/CGO as fuel electrode and $La_{0.58}Sr_{0.4}Fe_{0.8}Co_{0.2}O_{3-\delta}$ (LSCF) as air electrode on CGO-3YSZ-CGO substrates. These cells were characterized in steam electrolysis at 930°C by Electrochemical Impedance Spectroscopy (EIS). Further microstructural engineering and fine tuning of the manufacturing parameters are essential for a practical use of this electroctalyst for H_2O/CO_2 co-electrolysis operation.

Introduction

In the context of the energy transition, reuse of CO_2 from carbon-intensive processes is considered as promising scenario to defossilize human activity. By allowing simultaneous electrolysis of H_2O and CO_2, high temperature (above 800°C) Solid Oxide Electrolysis (SOE) enables direct production of syngas (H_2 + CO) that can, for instance, be converted downstream into valuable synthetic fuels and chemicals.

With respect to Solid Oxide Cells (SOC), state-of-the-art Ni-based fuel electrodes have been extensively studied due to their excellent electrical conductivity and high catalytic activity towards H_2O/CO_2 splitting at high temperature. However, they are vulnerable to poisoning, irreversible dimensional changes when alternating reducing and oxidizing operating conditions and microstructural instabilities that may occur at high

overpotentials (1). On one hand, in the case of the Ni-YSZ fuel electrodes, carbon formation has been identified at the electrode-electrolyte interface at high current densities and temperatures (~ 875°C) leading to microstructural changes and active site deactivation (2). Ni agglomeration has been also reported in such electrodes causing loss of electrical percolation and reduction of the triple-phase-boundary (TPB) length (3). On the other hand, Ni-CGO electrodes have been also studied as fuel electrode material due to their catalytic properties and superior tolerance to carbon formation (2). Nevertheless, due to large content of metallic nickel, Ni-CGO cermet electrodes are still vulnerable to dimensional alterations caused by microstructure coarsening upon redox cycling: after a cycle at 950°C, an increment on the conversion and diffusion impedances at 1 Hz were reported, assigned to an alteration of the gas transport processes, as well as an increase in ohmic resistance, correlated with a decrease in electronic conductivity (4).

As an alternative, perovskite-based oxides ABO_3 are promising materials for fuel electrodes in Solid Oxide Electrolysis Cells (SOECs) by virtue of their high stability in dual atmospheres, and tunable properties upon doping. High catalytic activity can be achieved when the *A*-site is a lanthanide and/or alkaline-earth cation and the *B*-site a transition metal cation, such as Mn, Co, Fe, Ni, Cr and Ti (5).

Lanthanum-strontium titanates (LST) have been recently studied by John T.S. Irvine's research group (JTSI Group – Energy and Materials in St Andrews). They have reported outstanding results on the performance of these materials as fuel electrode in steam electrolysis, by incorporating catalytically active nanoparticles on the surface of these perovskites, such as Ni and Fe nanoparticles (6). This was done by redox exsolution, whereby a catalytically active metal is substituted in the crystal lattice of the perovskite backbone in oxidizing conditions, and released (exsolved) on the surface as metal nanoparticles upon reducible atmosphere (7), although this process is limited by the stoichiometry. According to D. Neagu *et al.* exsolution takes place when the oxygen vacancies (induced by reduction) reach a high enough concentration in the presence of *A*-site vacancies, such that the perovskite lattice destabilizes due to high deficiency on two of its primitive sites and therefore will spontaneously exsolve from the *B*-site in order to re-establish the electro neutrality of the lattice (8).

This work presents the development of an *A*-site deficient lanthanum strontium chromite perovskite with 15% of Ni partial substitution on the *B*-site (LSCN) in order to decorate the surface with Ni nanoparticles by *in situ* exsolution. The presented results show the characterization of this electrocatalyst as well as its implementation as fuel electrode in an electrolyte-supported cell (ESC) with active surface area of 16 cm^2. Preliminary electrochemical characterizations were performed with the aim to identify the limiting manufacturing and operational parameters to be further optimized.

Experimental Procedures

LSCN precursor preparation

Perovskite formulations described in Table I were prepared by the sol- gel glycine nitrate combustion method (9). Firstly stoichiometric amounts of $La(NO_3)_2 \cdot 6\ H_2O$ (99.9% REO Alfa Aesar), $Sr(NO_3)_2$ (98% Alfa Aesar), $Ni(NO_3)_2 \cdot 6\ H_2O$ (98% Alfa Aesar), $Cr(NO_3)_2 \cdot 9\ H_2O$ (98.5% Alfa Aesar) and glycine (J.T.Baker™) were dissolved in

deionized water. The glycine molar ratio for the total content of metal cations was 2:1. Secondly the solution was stirred and heated on a hot plate at 220°C until self-combustion. The resulting powders were passed to a high temperature furnace and calcined in air up to 1400°C at a rate of 3K/min for one hour.

TABLE I. Abbreviation and composition of the different LSCN *A*-site deficient perovskite formulations.

Abbreviation	*La* deficiency on *A*-site (%)	Formulation
L70SCN	0	$La_{0.7}Sr_{0.3}Cr_{0.85}Ni_{0.15}O_{3-\delta}$
L65SCN	7	$La_{0.65}Sr_{0.3}Cr_{0.85}Ni_{0.15}O_{3-\delta}$
L60SCN	10	$La_{0.6}Sr_{0.3}Cr_{0.85}Ni_{0.15}O_{3-\delta}$
L50SCN	20	$La_{0.5}Sr_{0.3}Cr_{0.85}Ni_{0.15}O_{3-\delta}$

Precursor characterization

The produced LSCN powders were characterized by means of thermogravimetric analysis (TGA), differential scanning calorimetry (DSC), X – ray diffraction (XRD) and scanning electron microscopy (SEM). Rietveld refinement analyses were also performed with the intention to identify and quantify the phase with the final formulation of *La* deficient perovskite.

Thermal analysis. The analyzer Netzsch Jupiter 449C was used to perform TGA and DSC in synthetic air at a rate of 3K/min from 25°C to 1100°C.

Structural and morphological characterization. The crystalline structure was identified by XRD with a STOE diffractometer at 40 kV and 30 mA, with Co- Kα source and Bragg-Brentano configuration, at a range of 2θ from 20° - 90°, time step of 0.04 and scanning rate of 0.4°/min. Morphology and microstructure were observed with the scanning electron microscope Zeiss ULTRA PLUS SEM (Carl Zeiss AG, Germany).

Electrolyte Supported Cells (ESCs) fabrication

The electrolyte-supported cells were fabricated using commercial CGO20-3YSZ-CGO20 (Kerafol GmbH, Germany) substrates of square geometry (50 mm x 50 mm) and 90 μm of thickness. The air electrode was printed on one side of the substrates with a commercial ink of $La_{0.58}Sr_{0.4}Fe_{0.8}Co_{0.2}O_{3-\delta}$ (LSCF). On the opposite side, the fuel electrode ink L65SCN/CGO20 (50:50) was printed, which was prepared by dispersing these oxides in a solution of 94% α-Terpinol and 6% ethyl cellulose on a ratio of total powder to solution of 2:1. The printed surface for both electrodes was 16 cm^2 (40 mm x 40 mm). The cells were further fired at 1080°C in air at a rate of 3K/min for one hour.

Electrochemical testing

The electrochemical performance of the LSCN perovskite has been characterized at 930°C in steam electrolysis (and subsequently in co-electrolysis) operation with the test bench shown in Figure 1. Electrochemical Impedance Spectroscopy (EIS) has been performed in galvanostatic mode with the electrochemical workstation Zahner PP-240 at a frequency range from 50 mHz to 100 kHz. The amplitude of the current stimulus was

100 mA. Polarization curves still need to be done after optimizing the current collection of the manufactured ESC.

Test bench. The experimental setup for single cell testing has two main gas lines corresponding to fuel side and air side gases:

- Fuel side: CO, CO_2, N_2, H_2 and forming gas (95% N_2 – 5% H_2). Steam at 120°C is added downstream (after mixing the fuel side gases).
- Air side: air and O_2.

Figure 1. Test bench for high temperature electrolysis and co – electrolysis cell testing.

The cell was placed on an alumina cell holder of 100 mm diameter with 12 channels for the gas flow, in which the current and voltage supply wires are placed. To ensure the current collection, the fuel electrode was contacted with two coarse platinum meshes and one nickel fine mesh and the air electrode with one coarse and one fine platinum mesh and one gold fine mesh. A square gold frame of 300 – 400 μm of thickness was used to seal the cell during high temperature operation (~800-900°C), as shown in Figure 2.

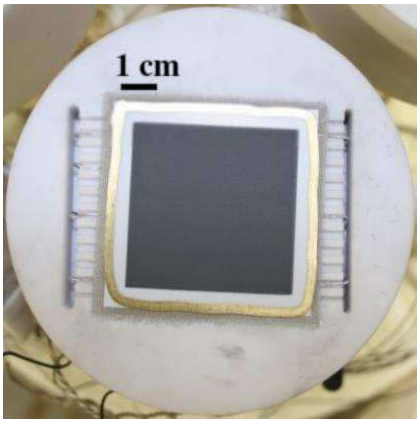

Figure 2. ESC placed on cell holder where the fuel electrode is faced down. The gold frame is used to seal tight the cell during operation.

Both fuel and air side gases were supplied to the cell from the center of the cell holder through the gas flow channels (passing through the meshes) in a co-flow configuration. Fuel gases were supplied from the bottom and air gases from the top of the cell holder. Additionally, 375g (5 weights of 75g each) were placed on the air side head in order to improve the contacting, as shown in Figure 3.

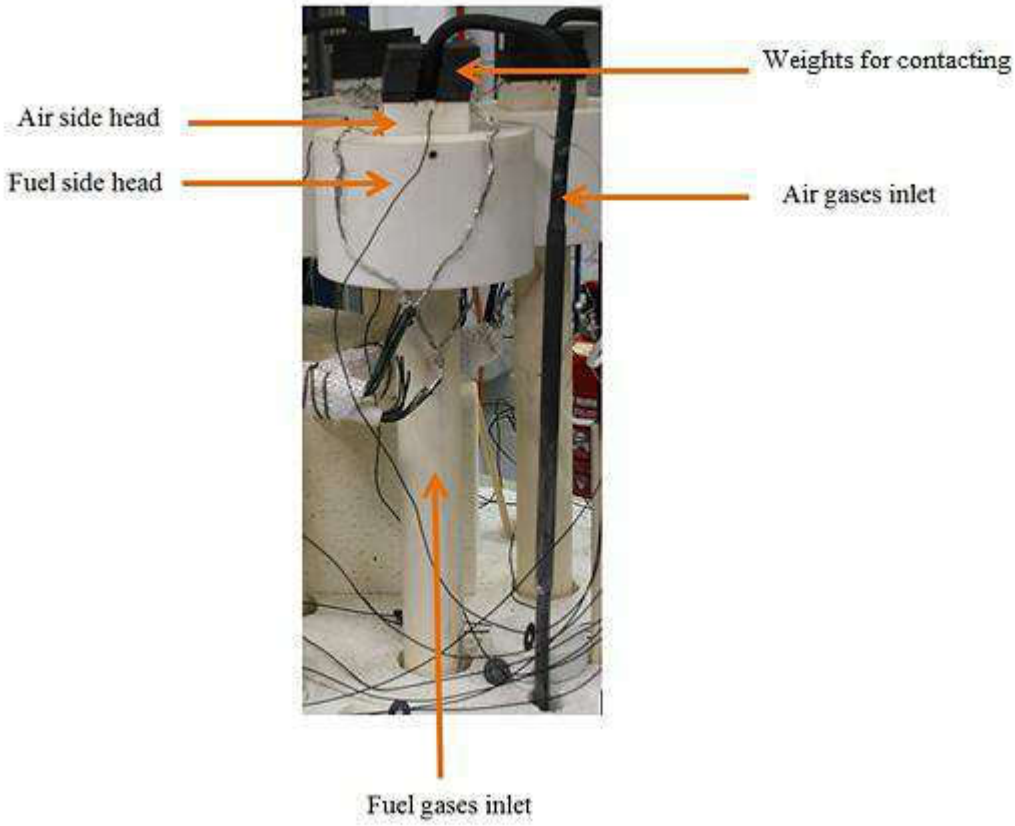

Figure 3. Cell holder on test bench, where fuel gases are fed from the bottom and air gases from above.

Results and Discussion

Preliminary results of the materials characterization, exsolution evidence and electrochemistry are presented in the following.

Characterization of materials

TGA and DSC in synthetic air for different precursors are shown on Figure 4. It is noticeable that the thermal behavior of the gel is nearly independent from the lanthanum stoichiometry, as all signals show a comparable evolution upon heating. Besides, it is possible to identify the solvent evaporation at ~ 91°C, followed by the exothermic self – combustion reaction of the formed gel at 224°C and finally from ~530°C the crystalline perovskite phase started to form. The latter could be explained because no mass is lost from this point, but some chemical reactions took place, since the DSC signal shows for all the samples heat of reactions even at high temperatures. Performing XRD investigation after interrupted firing experiments of the gel revealed that pure perovskite phase could be achieved only by firing the precursor at 1400°C, where the perovskites L50SCN, L60SCN and L70SCN were obtained (Figure 5).

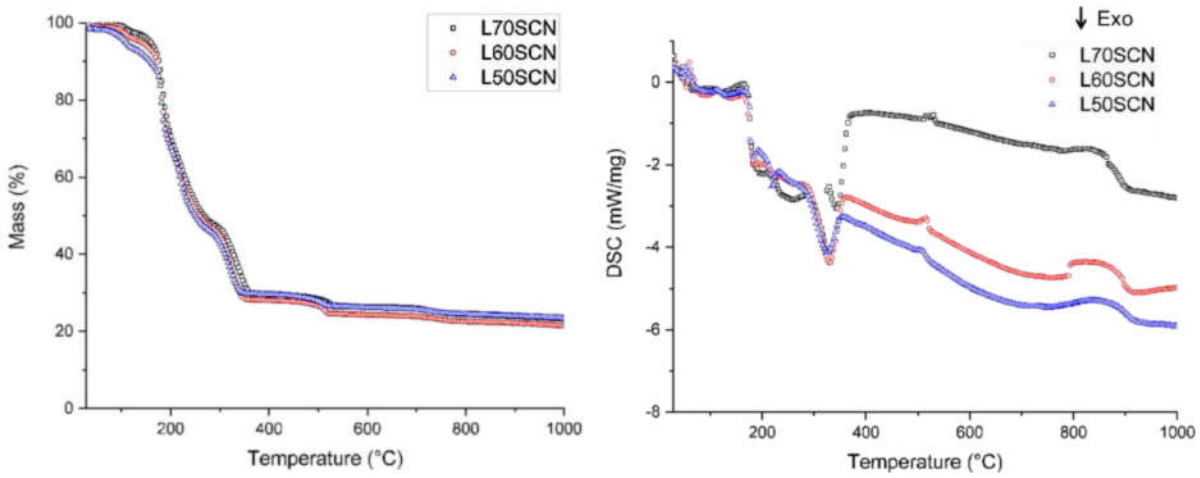

Figure 4. TGA (left) and DSC (right) in synthetic air for the formulations L50SCN, L60SCN and L70SCN.

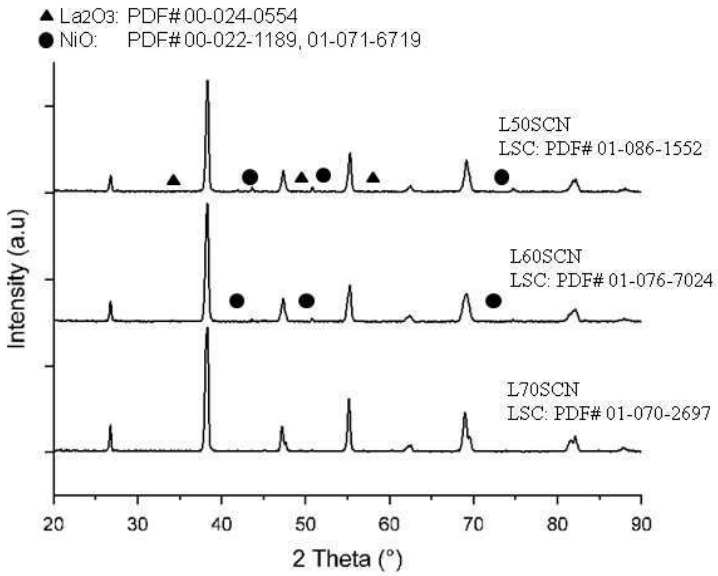

Figure 5. XRD patterns for the formulations L50SCN, L60SCN and L70SCN.

NiO impurities could be identified on the formulations with 10 and 20% of *La* deficiency. The latter exhibiting an additional phase identified as La_2O_3 which may strongly affect the performance due to the lack of electro-catalytic activities. Aiming at the synthesis of a pure single phase, this was deciding to formulate a *La* deficiency that yields to a perovskite phase without significant impurities that may affect performance. After synthesis, a thorough analysis of the perovskite with 7% *La* deficiency, namely L65SCN, by means of XRD and Rietveld refinement revealed single perovskite phase with a NiO content of less than 1% (~0.97%). (These results are not shown in this manuscript). Considering that this excess of NiO is turned *operando* into metallic nickel, and it is both catalytically active and electronically conductive, this low level of impurity can be tolerated and is not expected (considering the amount) to affect significantly the performance of the synthesized catalyst.

The morphology of the four different synthesized powders is shown on Figure 6. All the samples presented well-defined geometry particles (except for the sample L50SCN). The samples L70SCN and L65SCN presented a more homogenous particle size distribution compared to L60SCN and L50SCN. The latter showing a broader particle size distribution and additional round shape particles, which could be related to the traces of NiO and La_2O_3 that were found by XRD.

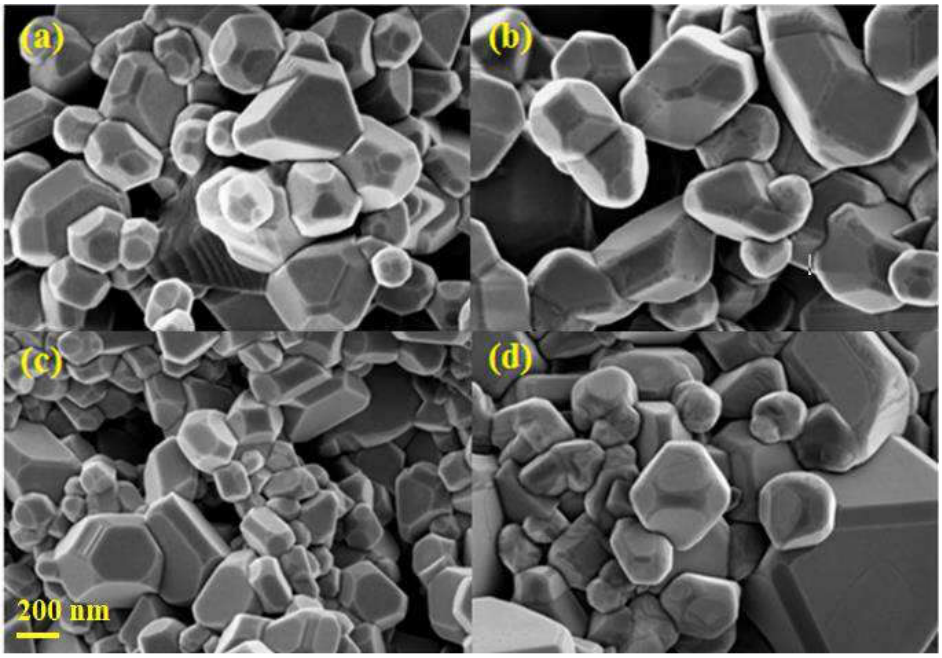

Figure 6. SEM images of powders L70SCN (a), L65SCN (b), L60SCN (c) and L50SCN (d).

On the basis of those investigations, L65SCN was selected as best candidate material in order to highlight Ni exsolution. This sample was exposed to a reducing atmosphere (5%H_2 – 95% N_2) up to 1200°C. SEM investigation of the treated powder revealed the presence of exsolved Ni nanoparticles of about 70-80 nm on the surface of the host perovskite L65SCN (Figure 7), which was confirmed by XRD and Rietveld refinement (not shown here). This demonstrates the potential of L65SCN as exsolution electrocatalyst for application in SOEC.

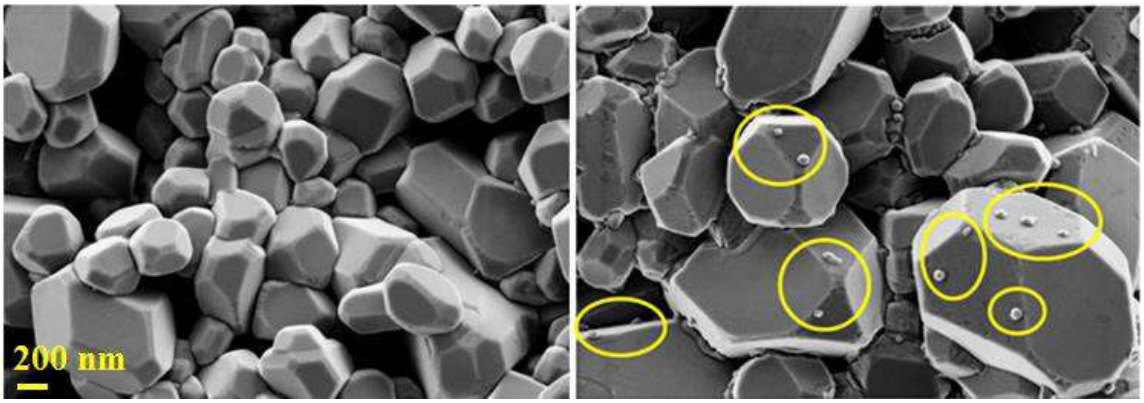

Figure 7. Left: SEM image of L65SCN powder before exsolution. Right: SEM image of L65SCN powder after exsolution of Ni nanoparticles (highlighted in yellow circles) at 1200°, under reducing atmosphere (5%H_2 – 95% N_2).

Electrochemical Impedance Spectroscopy (EIS)

Galvanostatic EIS was done at 930°C and 50% H_2O – 50% H_2 with the aim to perform an early assessment on steam electrolysis. The first characterization is shown in Figure 8, in which is noticeable that the ohmic resistance had a very high value (~7 Ω cm^2), which was speculated to be due to a poor current collection. For this reason, in an attempt to improve the current collection at the fuel electrode, silver paste was brushed on the L65SCN and dried in air at 550°C for 30 minutes. Furthermore EIS was repeated at the same conditions with the result on Figure 9.

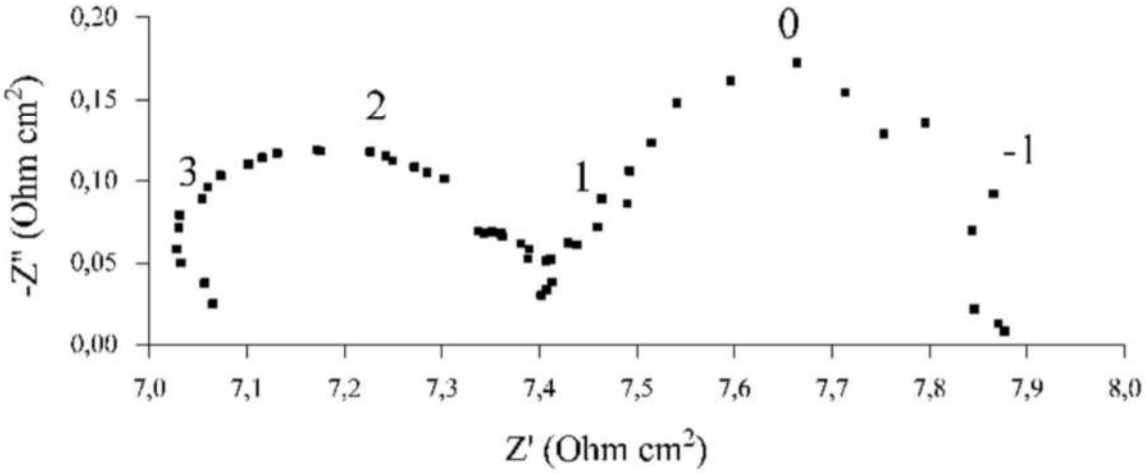

Figure 8. Nyquist plot of EIS spectra recorded at OCV, 930°C, 50% H_2O – 50% H_2.

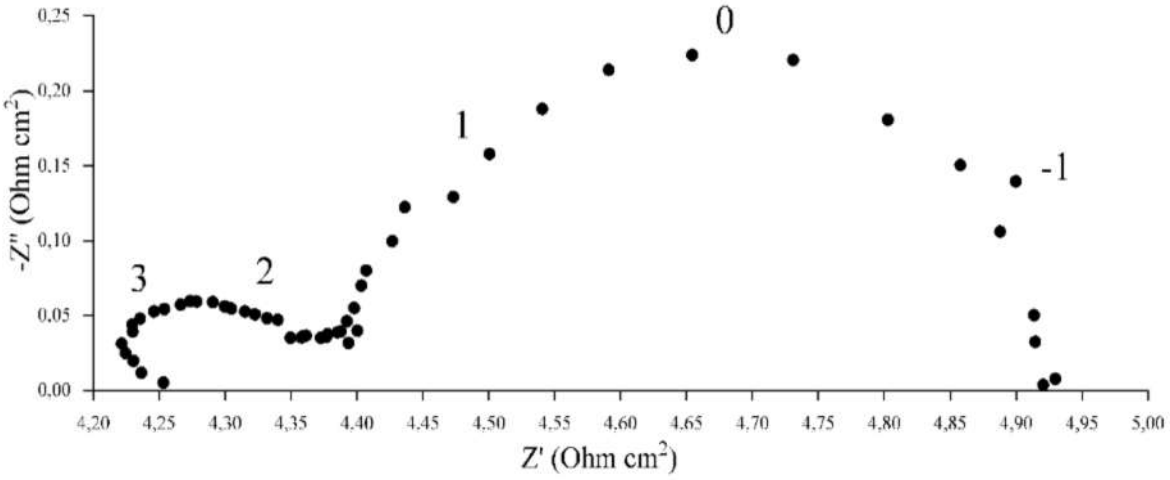

Figure 9. Nyquist plot of EIS spectra recorded at OCV, 930°C, 50% H_2O – 50% H_2 with silver paste on fuel electrode as current collection material

Upon contacting with a silver paste, the ohmic resistance was decreased from 7 to 4.25 Ω cm^2 and the spectra could be used to find the electrochemical parameters for modeling the steam electrolysis with the L65SCN as fuel electrode. This highlights the crucial role of the contacting to exploit perovskite based fuel electrodes. Nonetheless the

measured ohmic resistance is still very high in comparison to the one typically observed with commercial ESC implementing a Ni-CGO cermet (0.4 – 0.5 Ω cm^2).

After cooling, investigation of the cells revealed that large areas of both electrodes were delaminated (Figure 10). This is typically correlated with a significant increase of both ohmic and polarization resistances and may explain per part the large ohmic resistance despite the use of silver paste.

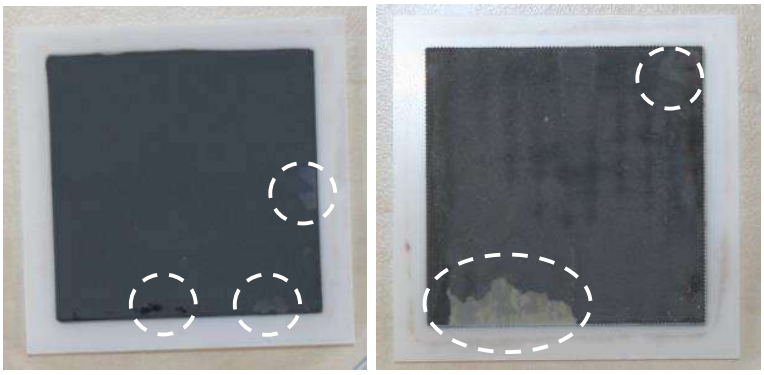

Figure 10. Delamination at the air electrode (left) and at the fuel electrode (right) after operation at OCV, 930°C, 50% H_2O – 50% H_2 with silver paste on fuel electrode as current collection material.

Conclusions and Outlook

In the present work different formulations of LSCN were investigated by varying the *A*–site deficiency on the Lanthanum content. It was found that the formulation L65SCN with 7% of this deficiency presented a pure perovskite phase with a NiO impurity of about 1%. Exsolution of Ni nanoparticles was confirmed on this composition after exposure to a slightly reducing atmosphere at 1200°C. Further investigations are required to optimize the exsolution parameters that will yield to a high electrocatalytic activity and performance. Besides, it is necessary to quantify how much Ni nanoparticles could be exsolved under stronger reducing environment. Parameters such as temperature, dwell time and Hydrogen partial pressure are expected to play a key role (6).

L65SCN was implemented as fuel electrode of an ESC, in which preliminary electrochemical characterizations were performed on steam electrolysis operation, revealing how the current collection affects in the performance of the fuel electrode. Furthermore, the observed delamination indicates that further engineering of the electrode (porosity, sintering temperature, and perovskite fraction) is required in order to achieve sufficient performance level for up-scaling and implementation into ESC stack.

Acknowledgments

The German Academic Exchange Service (DAAD) is acknowledged for the Ph.D. scholarship of Mrs. D.M. Amaya D. Part of this work has received support from the German Federal Ministry of Education and Research (BMBF) within the Kopernikus Project P2X (Grant n°03SFKE20).

References

1. M. P. Hoerlein, M. Riegraf, R. Costa, G. Schiller and K.A. Friedrich, *Electrochimica Acta*, **276**, p. 162-175, (2018).
2. V. Duboviks, R. C. Maher, M. Kishimoto, L. F. Cohen, N. P. Brandon and G. Offer, *J. RSC,***00**, p. 1-6, (2012).
3. T. L. Skafte, J. Hjelm, P. Blennow and C. Graves, in *12th European SOFC & SOE Forum 2016,* p. 8-27, Proceedings Series, Lucerne, (2016).
4. A. Faes, A. Hessler-Wyser, A. Zryd and J. Van herle, J. *Membranes,* **2**, p. 585-664, (2012).
5. H. Zhu, P. Zhang and S. Dai, *J. ACS Catal.,* **5**, p. 6370-6385, (2015).
6. G. Tsekouras, D. Neagu and J. T. Irvine, J. *Energy Environ. Sci.,***6**, p. 256-266, (2013).
7. J.H. Myung, D. Neagu, D. N. Miller and J. T. Irvine, **537**, *Nature,* p. 528-531, (2016).
8. D. Neagu, T.-S. Oh, D. N. Miller, H. Ménard, S. M. Bukhari, S. R. Gamble, R. J. Gorte, J. M. Vohs and J. T. Irvine, *Nature Commun.,* **6**, 8120, (2015.)
9. Y. Sun, J. Li, Y. Zeng, B. S. Amirkhiz, M. Wang, Y. Behnamian and J. Luo, *J. Mater. Chem. A,* **3**, p. 11048-11056,(2015).